**Supplementary Information for**

# Surfactant-free $NaBH_4$-mediated synthesis of $Au_xPd_{1-x}$ nano-alloys for active electrocatalysts

Kristian Junker Andersen,[a] Armin Asghari Alamdari,[a] Aleksandra Smolska,[a] Nina Lock,[a] Anders Bentien,[a] Jonathan Quinson*[b,a]

a) Biological and Chemical Engineering Department, Aarhus University, 40 Åbogade, 8200, Aarhus, Denmark
b) CICA-Centro Interdisciplinar de Química e Bioloxía, Facultade de Ciencias, Universidade da Coruña, Campus de Elviña, A Coruña, Spain

**Table S1**. Examples of reports where a surfactant-free $NaBH_4$-mediated in water solution was used to prepare nanomaterials.

| Ref. | Date | Metal | Type of NPs | Size nm | Precursor | [Precursor] $mM_{metal}$ | $NaBH_4$/Au Molar ratio | Volume mL | Catalysis |
|---|---|---|---|---|---|---|---|---|---|
| 1 | 1998 | Ag | Spheres | 10 | $AgClO_4$ | 0.125<br>0.250<br>0.500 | 3, 6, 12 | 200<br>100<br>50 | - |
| 2 | 2014 | Au | Spheres Networks | 5-100 | $HAuCl_4$ | 0.13 | 2-100 | 33 | 4-NP |
| 3 | 2016 | Au | Spheres | 5-10 | $HAuCl_4$ | 0.25 | 11-46 | N/S | - |
| 4 | 2023 | Au | Spheres | 5.6 | $HAuCl_4$ | 0.17 | 2-50 | 15 | 4-NP |
| 5 | 2025 | Au | Spheres | 3-8 | $HAuCl_4$ | 0.25 | 10 | 10 | - |
| 6 | 2025 | Au | Spheres | 5-20 | $HAuCl_4$ | 0.50 | 1-30 | 2 | - |
| 7 | 2025 | Au | Spheres | 5-15 | $HAuCl_4$ | 0.50 | 5-11 | 2 | 4-NP |
| 8 | 2025 | Au | Spheres | 4-20 | $HAuCl_4$ | 0.50 | 5-11 | 2, 100 | 4-NP, EOR |
| 9 | 2025 | Au | Spheres | 4-10 | $HAuCl_4$ | 0.10-0.50 | 5-10 | 2, 1000 | 4-NP, EOR |
| 10 | 2015 | Pd | Spheres Networks | < 5 | $K_2PdCl_4$ | 0.25 | 6 | 10-250 | N/A |
| 11 | 2023 | Pd | Spheres Network | 8 | $K_2PdCl_4$ | 13.6 | 0.67 | 11 | EOR |
| 12 | 2015 | Au, Ag, Pd, Pt, Rh, Cu | * | - | $HAuCl_4$, $AgNO_3$ $Pd(NO_3)_2$, $H_2PtCl_6$ $RhCl_3$, $CuSO_4$ ** | 0.5 (0.125-1.000) | 6 | - | - |
| 13 *** | 2016 | Ru | Network Chains | 3 | $RuCl_3$ | 0.61-5 | 0.5-4 | - | 4-NP, 4-NA, 2-SP, 2-NA, 4-NS, 2-B-6-NT, OER |
| 14 | 2023 | Pt | Network | 1-5 | $H_2PtCl_6$ | 0.13 | 10 | 20+ | redox reaction of $Fe(CN)_6^{3-}$ and $S_2O_3^{2-}$ $H_2O_2$ decomposition |
| 15 | 2019 | $Au_xAg_{1-x}$ | Spheres Networks | < 10 | $HAuCl_4$ $AgNO_3$ | 0.25 | 2- 10 | 20 | 4-NP |
| **This work** | 2026 | $Au_xPd_{1-x}$ | Spheres Networks | 5-15 | $HAuCl_4$ $Pd(NO_3)_2$ | 0.50 | 5 | 7 | EOR |

* the work only reported SAXS and it is not clear what shape the NPs have. It is confirmed that the materials are not stable as colloids.

** Other precursors of the same metals were used. *** Not at room temperature (35, 45, 60 °C).

4-nitrophenol (4-NP), 4-nitroaniline (4-NP), 4-nitrostyrene (4-NS), 2-nitrophenol (2-NP), 2-nitroaniline (2-NA), 2-bromo-6-nitrotoluene, (2-B-6-NT), oxygen evolution reaction (OER), ethanol oxidation reaction (EOR).

# 1- Synthesis

### 1.1. Chemicals

All chemicals were used as received: $HAuCl_4 \cdot 3H_2O$ (≥99.9%, Sigma-Aldrich); $Pd(NO_3)_2$ (> 99.0%, Merck) $NaBH_4$ (ReagentPlus®, 99%, Sigma-Aldrich); ultrapure water (mQ, Milli-Q, Millipore, resistivity of >18.2 MΩ•cm); HCl (puriss. ACS reagent, reag. ISO, Reag. Ph. Eur. fuming, ≥ 37%, Sigma Aldrich); $HNO_3$ (puriss ≥ 65%, Sigma Aldrich); ethanol (Absolute, ≥99.8%, AnalaR NORMAPUR® ACS, Reag. Ph. Eur. analyse reagens, VWR); KOH (Reag. Ph. Eur., VWR).

Extra caution was taken so that none of the chemicals was in contact with metal (e.g. metallic spatulas were not used and plastic spatulas were preferred). Dispose of chemicals following local rules. Pay attention to HCl, $HNO_3$ and $NaBH_4$ wastes.

### 1.2. $Au_xPd_{1-x}$ synthesis

The general synthesis follows the method proposed by Astruc and co-workers,[2] with adaptations. To an aqueous solution of $HAuCl_4$ and $Pd(NO_3)_2$ in water with molar ratio of 100:0, 99:1, 90:10, 80:20, 70:30, 60:40, 50:50, 40:60, 30:70, 20:80, 10:90, 1:99 and 0:100, $NaBH_4$ is added under vigorous stirring (here, 1500 rpm). In the present study, the synthesis was performed in glass vials (clean with boiling mQ water prior to use), de-dusted with a gentle flow of compressed air before being used. The magnets used for stirring are PTFE cylindrical stirrer bar (8 x 3 mm), cleaned with *aqua regia* (4:1, v:v, HCl:$HNO_3$; ***to be handled and disposed of with care following the related safety procedures in place in the laboratory***), washed with copious amount of water, and de-dusted prior to use. The chemicals were added in a mixture of water, $HAuCl_4$ and $Pd(NO_3)_2$, stirred for at least 5 minutes and finally $NaBH_4$ (under stirring). All solutions were prepared using ultrapure (mQ) water.

The stock solutions were 10 mM of $HAuCl_4$, 10 mM $Pd(NO_3)_2$, and 100 mM of $NaBH_4$. The stock solution of $HAuCl_4$ and $Pd(NO_3)_2$ was kept in a fridge at 5 °C, whereas the stock solutions of $NaBH_4$ was prepared freshly and used within 30 minutes of preparation. $NaBH_4$ was added under stirring, and the solutions capped after adding $NaBH_4$ and left to stir at room temperature for ca. 10 minutes (although the reaction proceeds in seconds). The total volume of solution was 7 mL in all cases. Afterwards the magnets were removed and the samples sealed with Parafilm®. The samples were then stored at room temperature in drawers. To minimize the effect of using different batches of $NaBH_4$, all experiments were prepared the same day with the same batch.

The concentrations of metal (e.g. Au) is typically 0.1-0.5 mM in the literature to lead to successful syntheses. At higher concentrations, the NPs tend to agglomerate. Here a total metal concentration of 0.5 mM was used for all experiments. The $NaBH_4$/Metal molar ratio of 5 was here selected because it was found to be optimal to minimize the amount of $NaBH_4$ to use and at lower values to yet obtain stable Au NPs (taking Au NP recipe as reference here).[6]

***Miscellaneous***

For transparency, we stress that the reaction were performed in a photo-box (Puluz LED portable Photo Studio, PU5060EU, 60 cm x 60 cm x 60 cm, 60 W) that we use for other syntheses in our research facilities to control light environment,[12,13] although we did not observe any an influence of the light environment on the $NaBH_4$-mediated synthesis.

# 2- UV-vis

UV-vis measurements were performed using a Shimadzu UV-1800 UV/Visible scanning spectrophotometer. The solutions were measured as prepared in a 1 cm width polystyrene squared shape UV-vis cuvettes. As baseline, mQ water was used since none of the chemicals considered absorb in the range of wavelengths considered. Details on the plasmonic signatures of Au NPs can be found elsewhere.[16]

# 3- STEM-EDS

STEM micrographs were acquired on a FEI Talos F200X operated at 200 kV STEM with a high-angle annular dark-field (HAADF) detector. The as-prepared colloidal dispersions were redispersed for 2 minutes by sonication, then dropped on copper TEM grids (Sigma-Aldrich) and washed with water. The samples were characterized by imaging at least 3 randomly selected areas at 3 different magnifications.

The size analysis was performed using a python package named NP-SAM used for segmentation and characterization of spherical NP, the segmentation was evaluated and improbable segments removed.[17] The nanostructures with predominant network morphology were measured using ImageJ, taking the thickness of the wire sub-structure of the network structure. The number of counts are indicated in each case. For EDS and estimation of the composition was based on the L lines from at least 3 different areas, group of NPs or individual NPs.

# 4- XRD

XRD measurements were performed using a Panalytical Aeris diffractometer operating in Bragg-Brentano mode with a PIXcel1D detector. Cu Kα radiation ($K\alpha_1$ = 1.54056 Å, $K\alpha_2$ = 1.54439 Å) was applied at 40 kV and 15 mA. Diffraction data were recorded between 5° and 90° (2θ), with a collection time of 600 minutes per sample. For Au-Pd samples, 1 mL of dispersion was applied to a silicone holder and oven-dried at 45 °C. This step was repeated once, after which the dried sample was repeatedly treated with ethanol to eliminate non-metallic residues. The sample was oven-dried at 45 °C before XRD analysis.

Phase composition was determined by matching experimental patterns with reference data for Au and Pd. The corresponding patterns XRD patterns for Au-Pd samples are presented in **Figure S5** below. Due to low metal loading and the small size of the nanomaterial and nanoscale samples, the diffraction peaks are generally weak and poorly resolved and the data had to be filtered (using adjacent averaging) using different points of window for each sample. Among the observed features, a broad reflection, centered around 2θ = 38° can be identified, which can be assigned to the (111) plane of face-centred cubic (fcc) Au or Pd. When comparing the patterns with decreasing Au content and increasing Pd content, a gradual shift of this reflection toward higher 2θ values is observed. This shift is consistent with the increasing Pd content, which characteristic fcc (111) reflection occurs at higher angles than that of Au. Higher-order reflections are not clearly resolved, likely due to peak broadening and low overall metal concentrations.

# 5- Electrochemistry

The EOR is a reaction relevant for energy conversion in alcohol fuel cells.[18] The general procedure previously reported was followed. [18] A three-electrode set up composed of a glassy carbon (GC) working electrode (WE ) with a diameter of 5 mm (0.2 $cm^2$), a graphite rod (Thermo Scientific Chemicals, 6.15 mm x 152 mm, 15403735) counter electrode (CE), and a Hg/HgO (Origalys, OGR001), electrode as reference electrode (RE), as indicated, immerged in ca. 20 mL of electrolyte in a Pyrex container.

The WE was prepared by dropping and letting dry overnight at room temperature 10 µL of the as-prepared dispersions of $Au_xPd_{1-x}$ NPs (0.5 $mM_{Au+Pd}$, sonicated for 2 minutes before sampling the colloids), on the GC surface (polished to mirror finish using aluminum polishing slurry, 0.30 and 0.05 µm alumina, eDAQ), making a 'tip'. All the electrochemical experiments were conducted using a computer-controlled potentiostat (Eci-100, NordicElectrochemistry) at room temperature (ca. 22 °C). We previously observed that the reaction is not mass transport limited and therefore no rotation was used. The electrolytes were not purged with $N_2$ or any other gases to mimick conditions closer to those of a direct alcohol fuel cells. The voltage expressed versus the Hg/HgO ($V_{Hg/HgO}$) electrode was converted to $V_{RHE}$ by the relationship: $V_{RHE} = V_{Hg/HgO} + 0.992$ (in V) in 1 M KOH.[19]
There are no commonly agreed on procedures to tests catalysts for the EOR and different scan rates, electrolytes, electrolyte concentrations, amounts of catalyst, upper and lower potentials are reported cross the literature,[18,20] not to mention the different normalizations reported. Here, each sample was tested following the same protocol for at least three different tips of the same $Au_xPd_{1-x}$ NPs obtained from the same synthesis conditions. The mass activity (MA) was evaluated by cyclic voltammetry (CV) assuming a total conversion of the $Au^{III}$ to $Au^0$ and $Pd^{II}$ to $Pd^0$ and using at least 2 values for average and standard deviation.

The electrochemical characterization consisted of CV and chromoamperometry (CA). For CVs, 50 scans at 50 mV $s^{-1}$ in 1 M KOH and 1 M Ethanol between -0.80 and 0.50 $V_{Hg/HgO}$ (0.20–1.50 $V_{RHE}$) were performed. The MA was evaluated as the higher oxidative current retrieved using the 50$^{th}$ scan. For chronoamperometry the potential was hold for 1 hour at -0.10 or 0.20 $V_{Hg/HgO}$ (0.9 or 1.2 $V_{RHE}$), as indicated, in the same electrolyte.

### *Note*

As opposed to our previous work, we did not attempt here to evaluate the electrochemically active surface area (ECSA) that can be challenging for a multimetallic NPs with both Au and Pd sites.[20] A preference is given to the MA: (i) To take into account the overall amount of metal used in the synthesis (cost-weighted activity, where the cost here will come from the amount of $HAuCl_4$ and $Pd(NO_3)_2$ used, regardless of the overall yield). (ii) To minimize steps between Au NP synthesis and catalytic screening, no isolation / washing / processing of the NPs, or no supporting on conductive materials such as high surface area carbon, for a direct use of the as-produced colloids, alleviating here from possible support effects and allowing a faster screening.

### *Metrics*

An illustrative CV of the EOR catalyzed by $Au_xPd_{1-x}$ samples is proposed in **Figure S6** below. In addition to the MA, the $I_f/I_b$ (explained along **Figure S6**) that correspond to the ratio of the peak intensity of the maximum of the forward and backward scans in CV, is commonly used to evaluate the poisoning resistance of the material, as detailed elsewhere.[21-23]

# 6- Results

**a)**

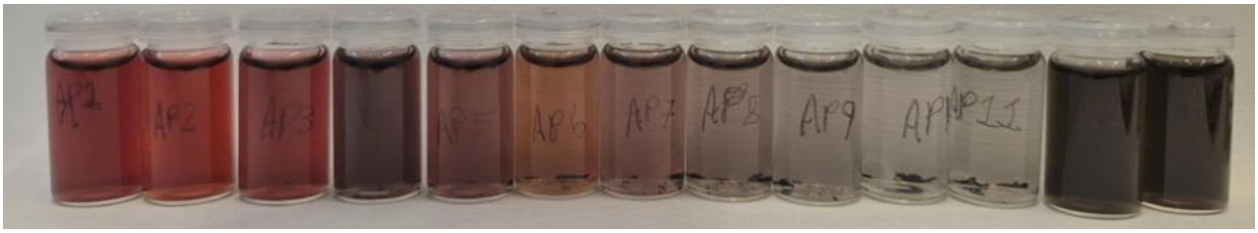

**b)**

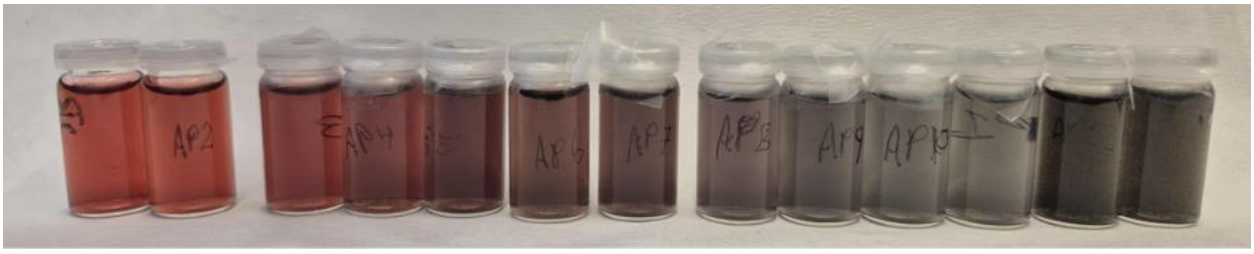

**Figure S1**. Illustrative pictures of the Au-Pd colloidal surfactant-free dispersions obtained in 7 mL of water using an $NaBH_4$-mediated synthesis. From left to right the nominal content of Au:Pd is: 100:00 (Au), 99:1 ($Au_{99}Pd_1$), 90:10 ($Au_{90}Pd_{10}$), 80:20 ($Au_{80}Pd_{20}$), 70:30 ($Au_{70}Pd_{30}$), 60:40 ($Au_{60}Pd_{40}$), 50:50 ($Au_{50}Pd_{50}$), 40:60 ($Au_{40}Pd_{40}$), 30:70 ($A_{30}Pd_{70}$), 20:80 ($A_{20}Pd_{80}$), 10:90 ($A_{10}Pd_{90}$), 1:99 ($A_1Pd_{99}$), 0:100 (Pd). The pictures were taken (a) 12 days after synthesis for samples stored at room temperature in a drawer, (b) 3.5 months after synthesis and after a sonication step for two minutes. The NPs are easily re-dispersed by sonication.

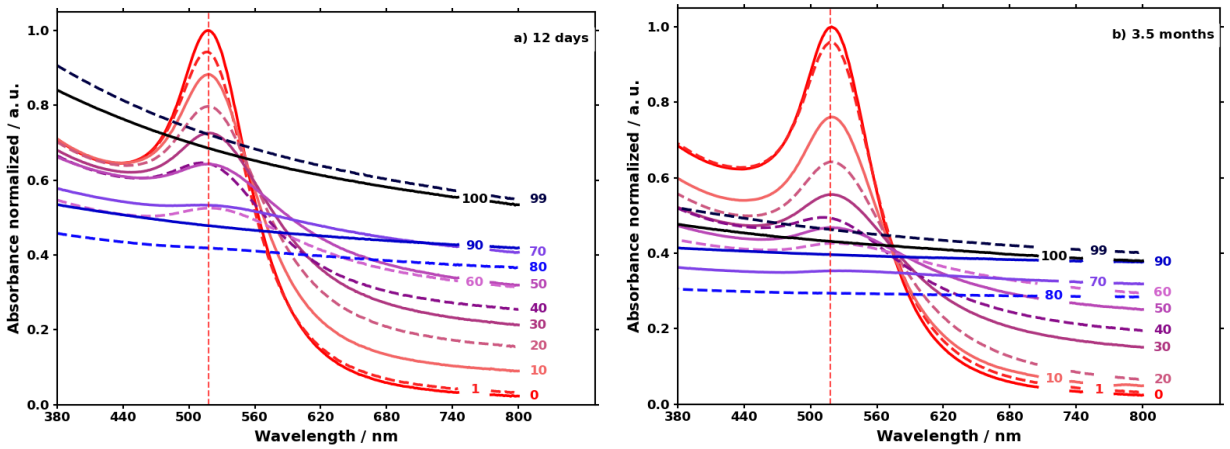


**Figure S2**. UV-vis spectra of the as prepared colloidal NPs (a) 12 days and (b) 3.5 months after synthesis and after sonication for re-dispersion. Panel (a) is the same as in the manuscript and reproduced here to facilitate the comparison.

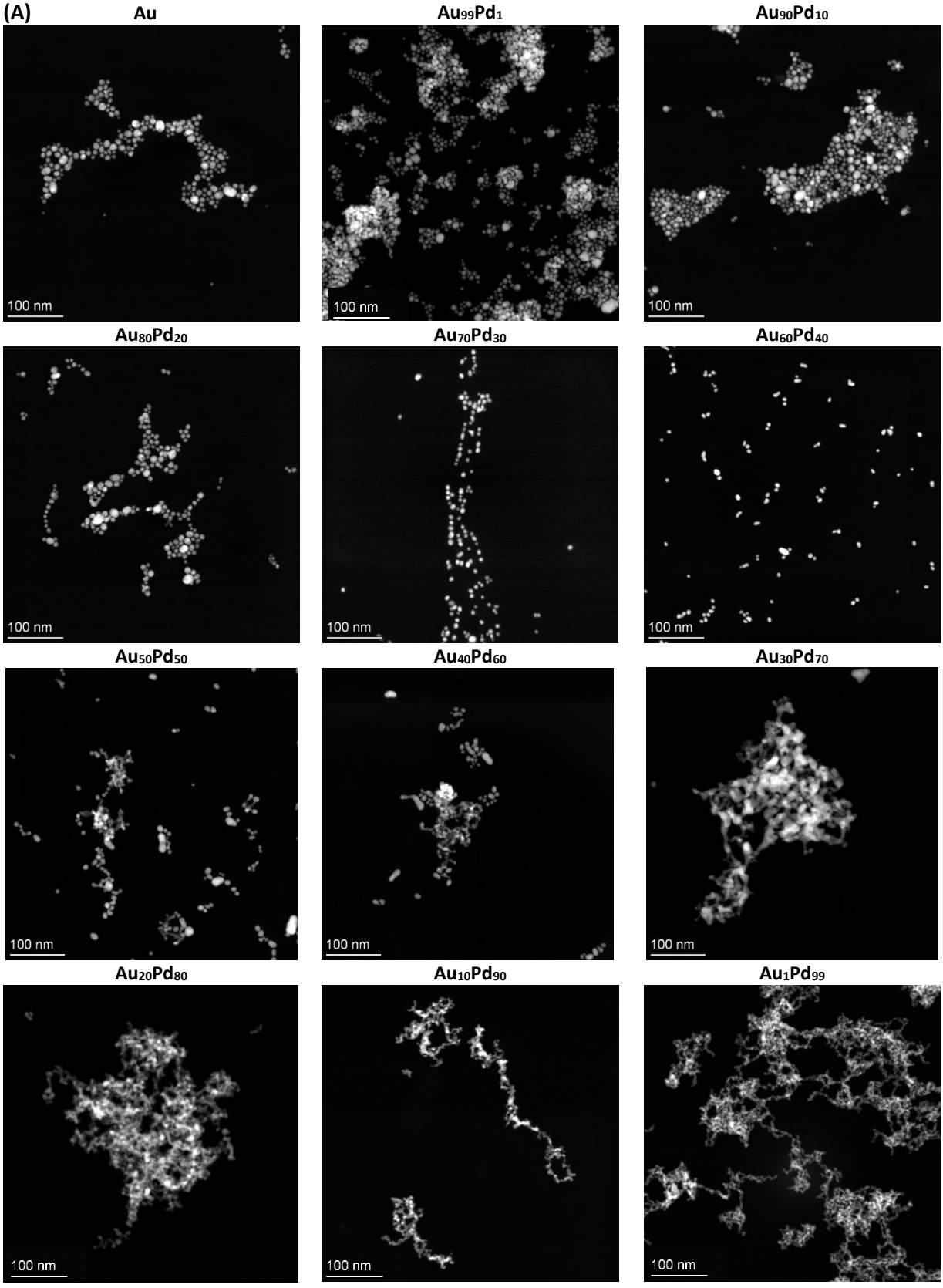
(A)
Au
Au99Pd1
Au90Pd10
Au80Pd20
Au70Pd30
Au60Pd40
Au50Pd50
Au40Pd60
Au30Pd70
Au20Pd80
Au10Pd90
Au1Pd99
100 nm

**Pd**

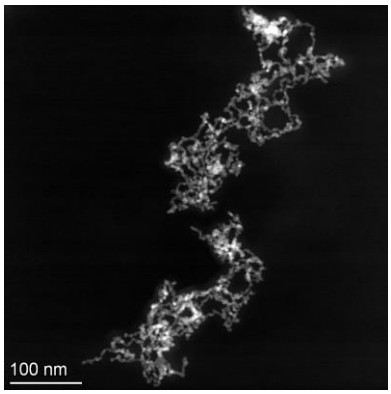


**(B)**

**Au**

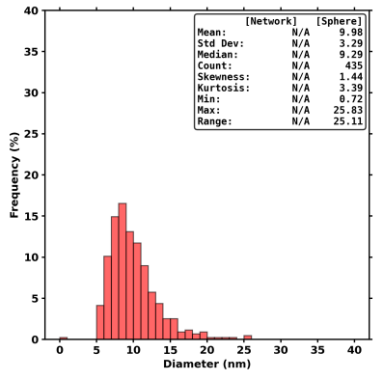


Sphere: 9.9 ± 3.3 nm (#435)

**$Au_{99}Pd_1$**

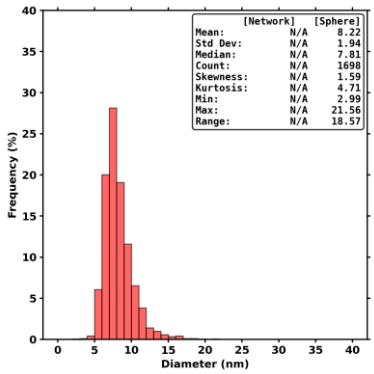


Sphere: 8.2 ± 1.9 nm (#1698)

**$Au_{90}Pd_{10}$**

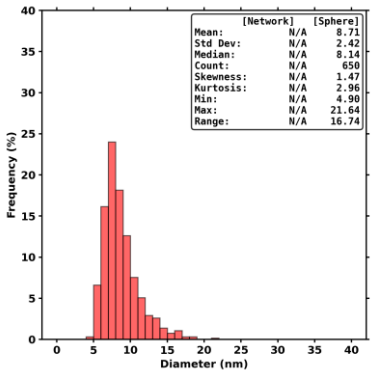


Sphere: 8.7 ± 2.4 nm (#650)

**$Au_{80}Pd_{20}$**

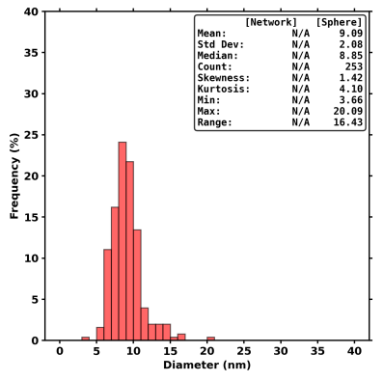


Sphere: 9.1 ± 2.1 (#253)

**$Au_{70}Pd_{30}$**

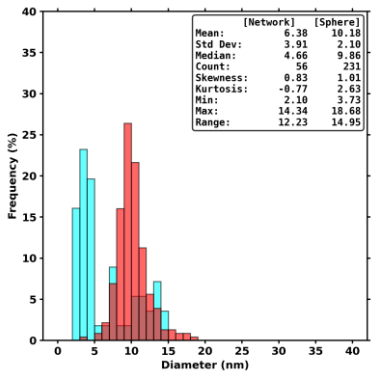


Sphere: 10.2 ± 2.1 nm (#231)
Network: 6.4 ± 3.9 (#56)

**$Au_{60}Pd_{40}$**

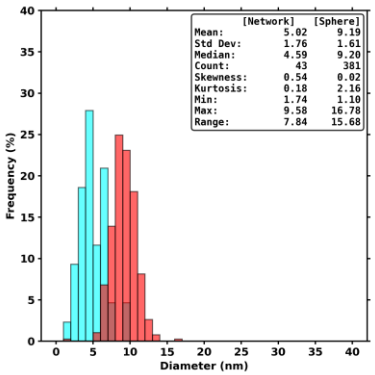


Sphere: 9.2 ± 1.6 (#381)
Network: 5.0 ± 1.8 (#43)

**$Au_{50}Pd_{50}$**

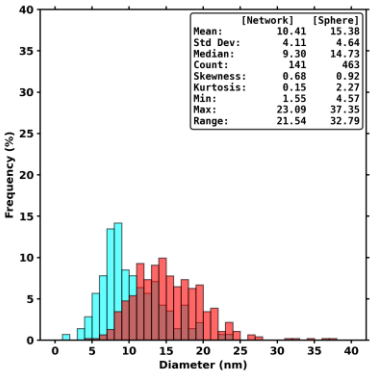


Sphere: 15.4 ± 4.6 (#463)
Network: 10.4 ± 4.1 (#141)

**$Au_{40}Pd_{60}$**

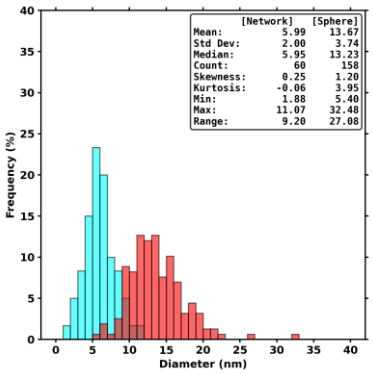


Sphere: 13.7 ± 3.7 (#158)
Network: 5.9 ± 2.0 (#60)

**$Au_{30}Pd_{70}$**

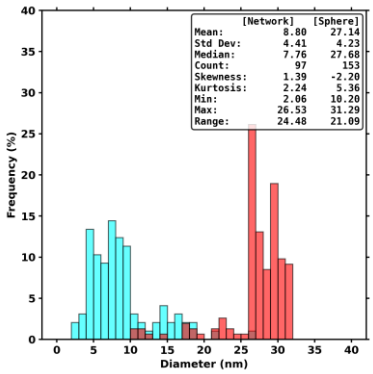


Sphere: 27.1 ± 4.2 (#153)
Network: 8.8 ± 4.4 (#97)

**$Au_{20}Pd_{80}$**

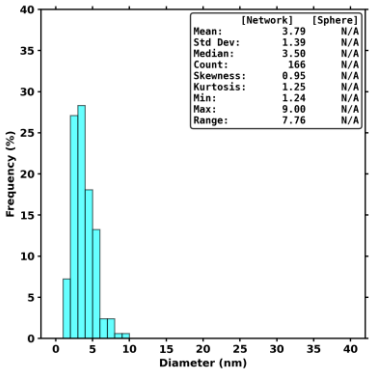


Network: 3.8 ± 1.4 (#166)

**$Au_{10}Pd_{90}$**

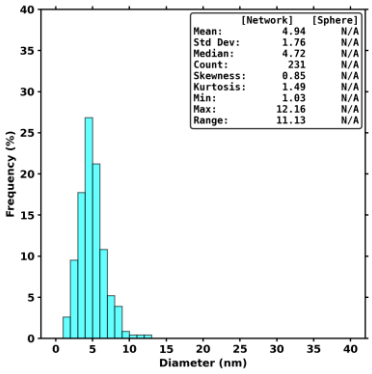


Network: 4.9 ± 1.8 (#231)

**$Au_{1}Pd_{99}$**

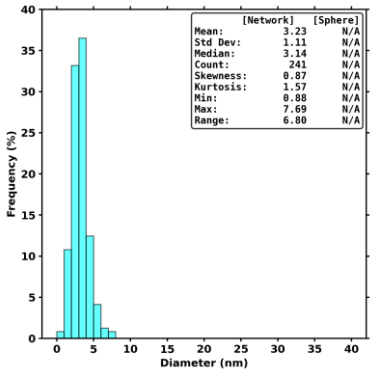


Network: 3.2 ± 1.1 (#241)

**Pd**

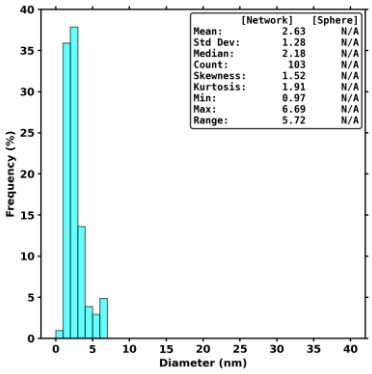


Network: 2.6 ± 1.2 (#103)

(C)

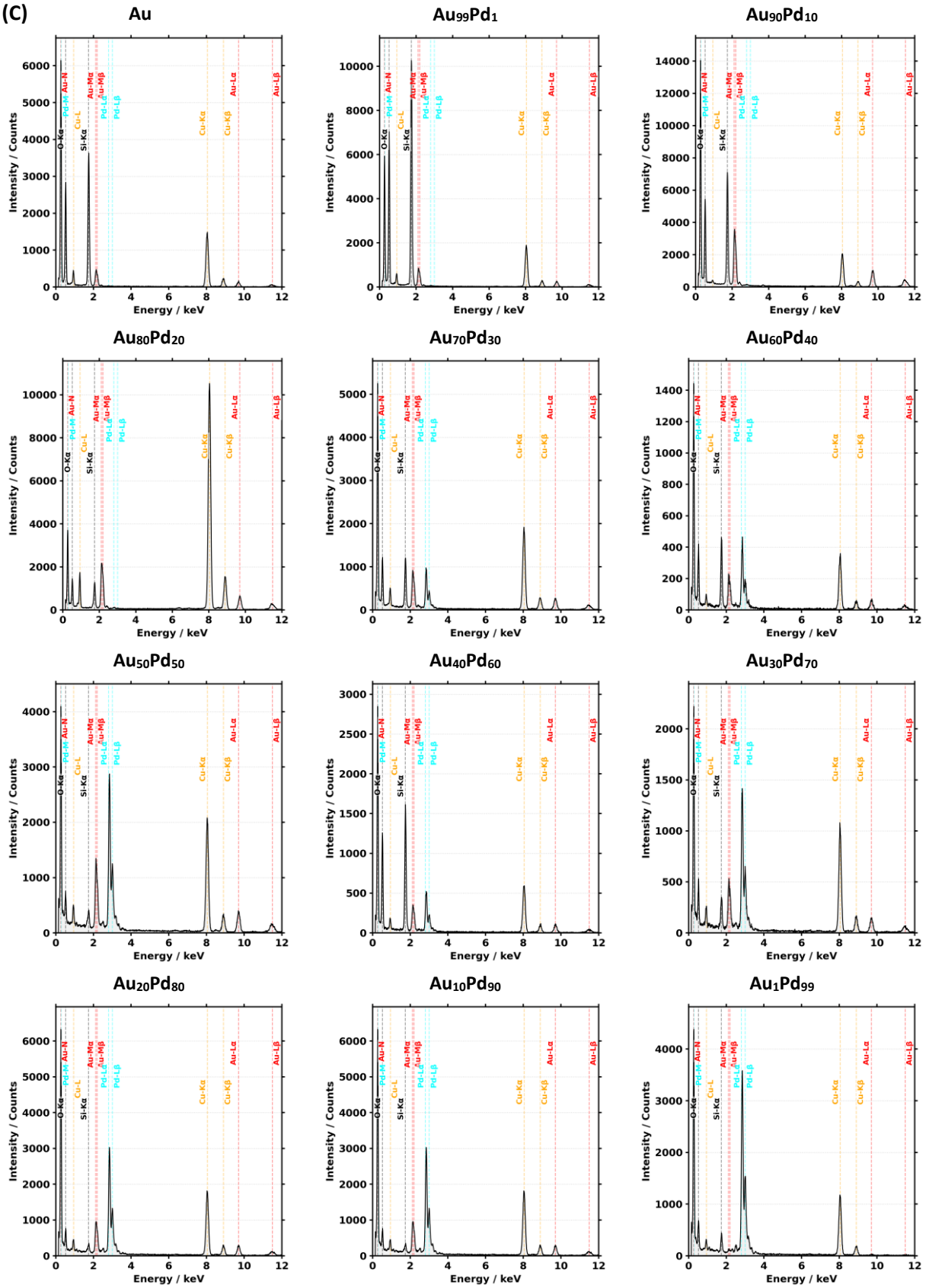
Au
Au99Pd1
Au90Pd10
Au80Pd20
Au70Pd30
Au60Pd40
Au50Pd50
Au40Pd60
Au30Pd70
Au20Pd80
Au10Pd90
Au1Pd99
Intensity / Counts
Energy / keV
O-Kα
Pd-Mζ
Au-N
Cu-L
Si-Kα
Au-Mα
Au-Mβ
Pd-Lα
Pd-Lβ
Cu-Kα
Cu-Kβ
Au-Lα
Au-Lβ

**Pd**

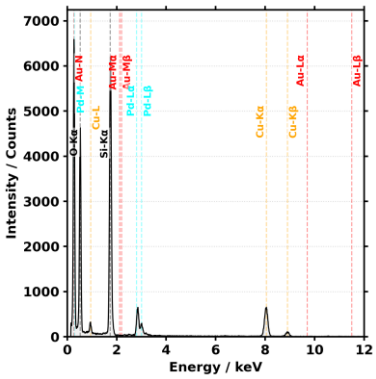


**(D)**

**Au**

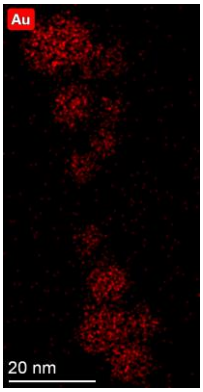


**$Au_{99}Pd_1$**

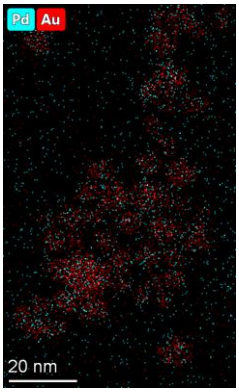


**$Au_{90}Pd_{10}$**

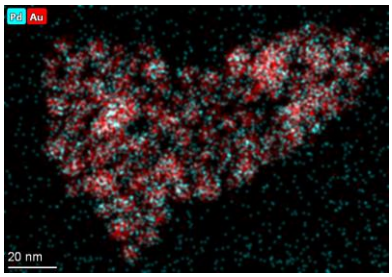


**$Au_{80}Pd_{20}$**

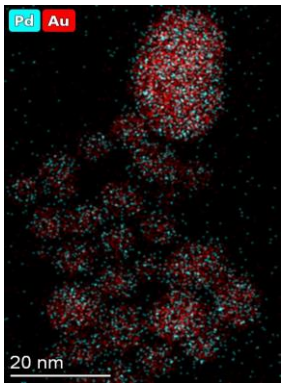


**$Au_{70}Pd_{30}$**

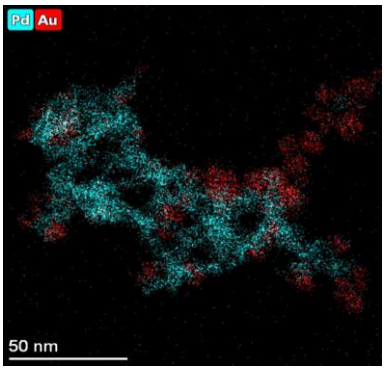


**$Au_{60}Pd_{40}$**

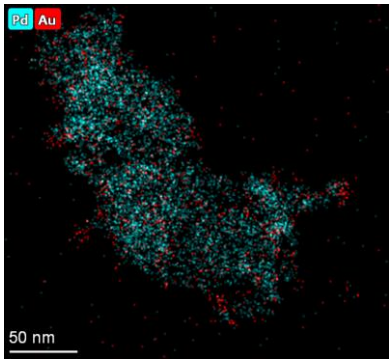


**$Au_{50}Pd_{50}$**

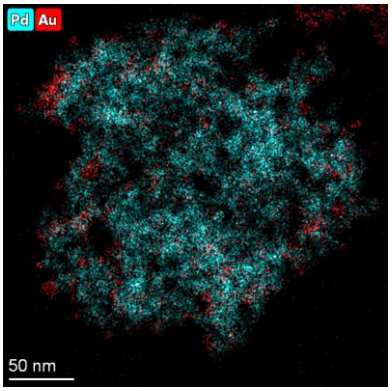


**$Au_{40}Pd_{60}$**

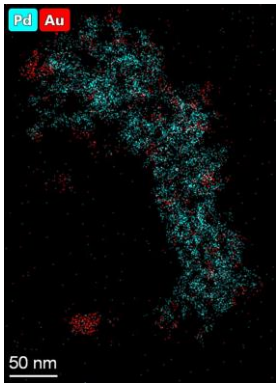


**$Au_{30}Pd_{70}$**

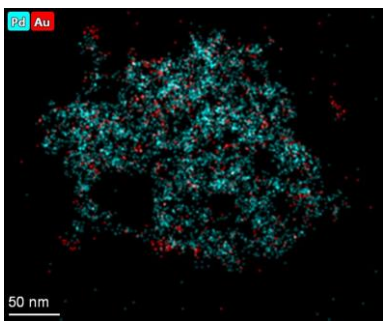

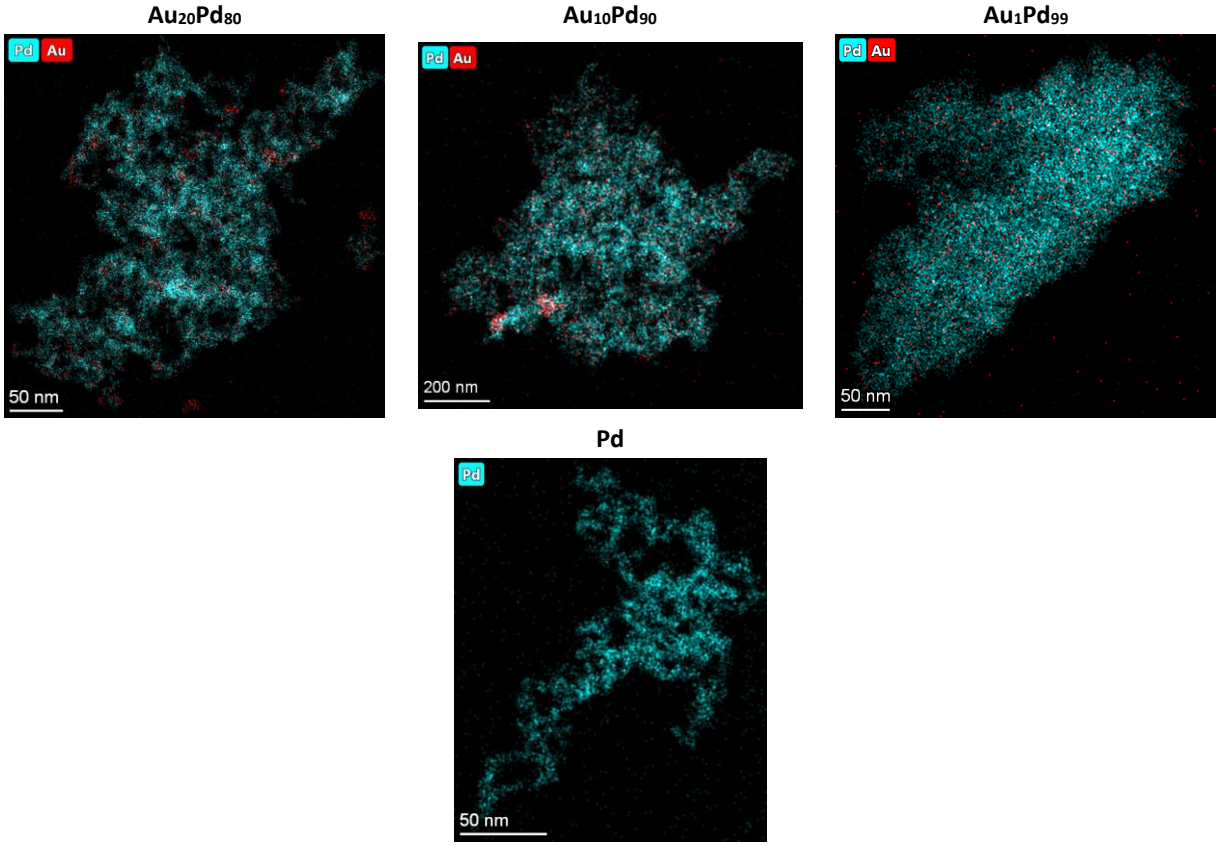


**Figure S3**. (A) Illustrative STEM micrographs for the different samples, as indicated. The micrographs were recorded at the same magnification. (B) Related size distributions. (C) Illustrative EDS spectra. (D) Illustrative EDS maps for the various samples, as indicated. The micrographs were recorded at different magnifications.

**a)**

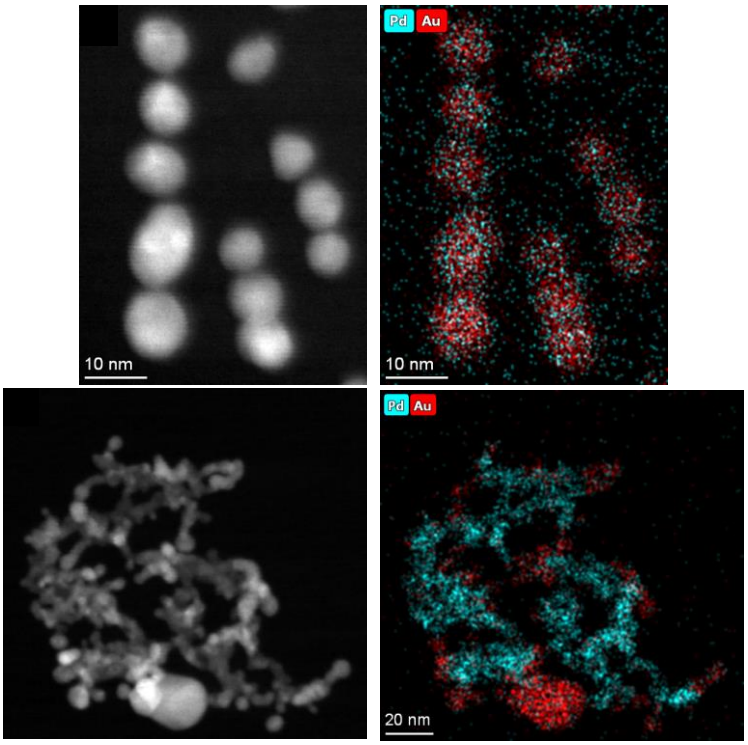


**b)**

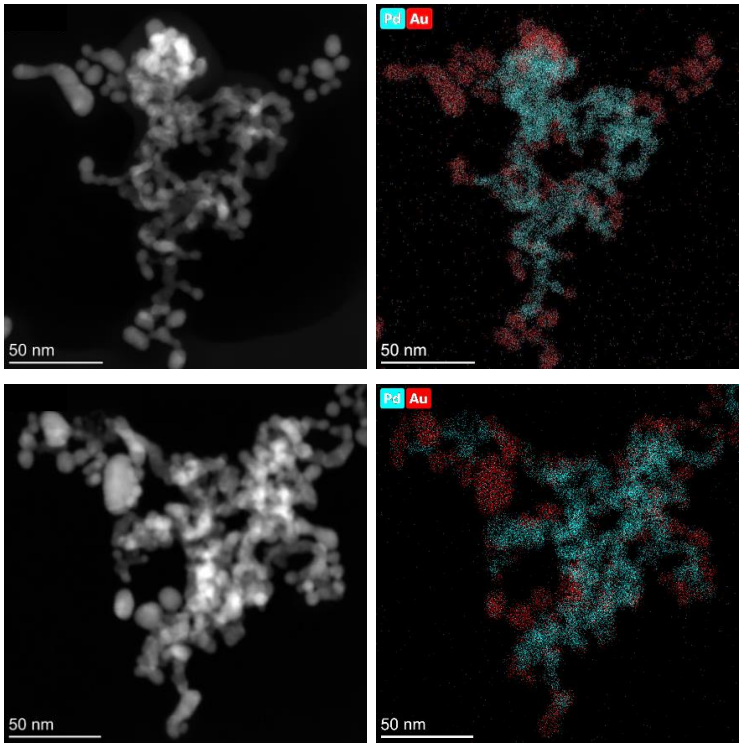


**Figure S4**. Illustrative STEM-EDS characterization (HAADF micrographs on the left and corresponding colored map on the right) of the (a) $Au_{70}Pd_{30}$ samples and (b) $Au_{40}Pd_{60}$ showing the Au-rich spherical materials and Pd-rich network-like materials within a same sample.

**Table S2**. Overview of the sample properties, including nominal and experimental EDS-retrieved composition, overall shape and size, lattice parameters and MAs.

| **Sample** | **Nominal composition** Au : Pd | **Average Experimental composition** Au : Pd EDS retrieved (deviation) | **Shape** | **Size** nm | **Lattice Parameter (a)** Å | **MA** 50$^{th}$ scans A g$^{-1}$ | **$I_f/I_b$** |
|---|---|---|---|---|---|---|---|
| Au | 100 : 00 | - | Spheres | 9.9 ± 3.3 | 4.124 | 272.5 ± 5.4 | 4.77 ± 0.44 |
| $Au_{99}Pd_1$ | 99 : 01 | 97.5: 2.5 (0.4) | Spheres | 8.2 ± 1.9 | - | 352.5 ± 5.3 | 4.65 ± 0.03 |
| $Au_{90}Pd_{10}$ | 90 : 10 | 96.4 : 3.6 (0.7) | Spheres | 8.17± 2.4 | - | 659.6 ± 229.8 | 1.09 ± 0.03 |
| $Au_{80}Pd_{20}$ | 80 : 20 | 95.6 : 4.4 (0.3) | Spheres | 9.1 ± 2.1 | 4.118 | 1221.0 ± 12.7 | 1.03 ± 0.00(3) |
| $Au_{70}Pd_{30}$ | 70 : 30 | 58.7 : 41.3 (31.2)<br>94.5 : 5.5 (0.3)<br>31.9 : 68.1 (5.2) | Spheres + Network | 10.2 ± 2.1<br>6.4 ± 3.9 | - | 1770.1 ± 1197.4 | 0.96 ± 0.11 |
| $Au_{60}Pd_{40}$ | 60 : 40 | 57.6 : 42.4 (37.1)<br>94.6 : 5.4 (3.4)<br>20.6 : 79.4 (1.6) | Spheres + Network | 9.2 ± 1.6<br>5.0 ± 1.8 | - | 2893.6 ± 65.4 | 0.92 ± 0.0004 |
| $Au_{50}Pd_{50}$ | 50 : 50 | 58.8: 41.2 (35.2)<br>90.3 : 9.7 (2.8)<br>19.6 : 80.4 (1.2) | Spheres + Network | 15.4 ± 4.6<br>10.4 ± 4.1 | 4.111 | 2757.6 ± 767.2 | 0.98 ± 0.03 |
| $Au_{40}Pd_{60}$ | 40 : 60 | 50.9 : 49.1 (34.1)<br>90.6 : 9.4 (3.5)<br>22.6 : 77.4 (7.8) | Spheres + Network | 13.7 ± 3.7<br>5.9 ± 2.0 | - | 3313.1 ± 147.4 | 0.95 ± 0.003 |
| $Au_{30}Pd_{70}$ | 30 : 70 | 50.6 : 49.4 (35.5)<br>86.0 : 14.0 (2.8)<br>15.2 : 84.8 (1.0) | Spheres + Network | 27.1 ± 4.2<br>8.8 ± 4.4 | - | 2966.5 ± 844.2 | 0.92 ± 0.003 |
| $Au_{20}Pd_{80}$ | 20 : 80 | 21.5 : 78.5 (13.1) | Network | 3.8 ± 1.4 | 4.000 | 4072.7 ± 46.3 | 1.12 ± 0.02 |
| $Au_{10}Pd_{90}$ | 10 : 90 | 7.7 : 92.3 (0.8) | Network | 4.9 ± 1.8 | - | 4430.0 ± 79.5 | 0.94 ± 0.09 |
| $Au_1Pd_{99}$ | 01 : 99 | 0.6: 99.4 (0.3) | Network | 3.2 ± 1.1 | - | 4257.1 ± 522.0 | 1.39 ± 0.003 |
| Pd | 00 : 100 | - | Network | 2.6 ± 1.3 | 3.992 | 3756.4 ± 375.4 | 0.85 ± 0.08 |

- The samples were not measured (mainly due to the little relevance of the measurement for Au and Pd only composition and the too close values of lattice parameters for several composition for the precision of the XRD data retrieved).

In cases where the samples showed two main populations, the composition of the Au-rich and Pd-rich populations are given in red and blue, respectively.

a)

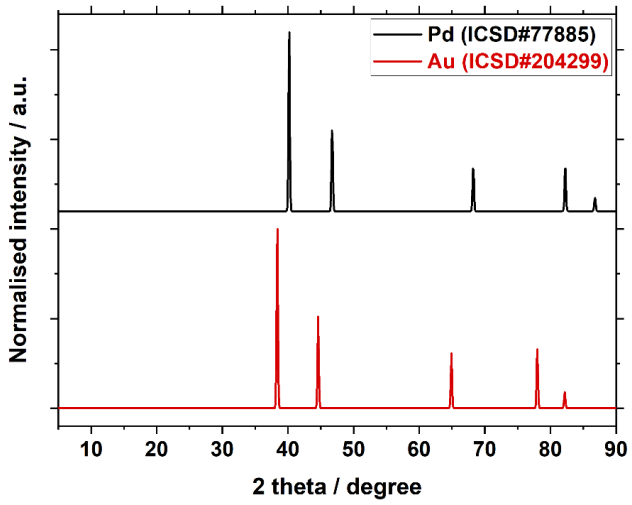


b)

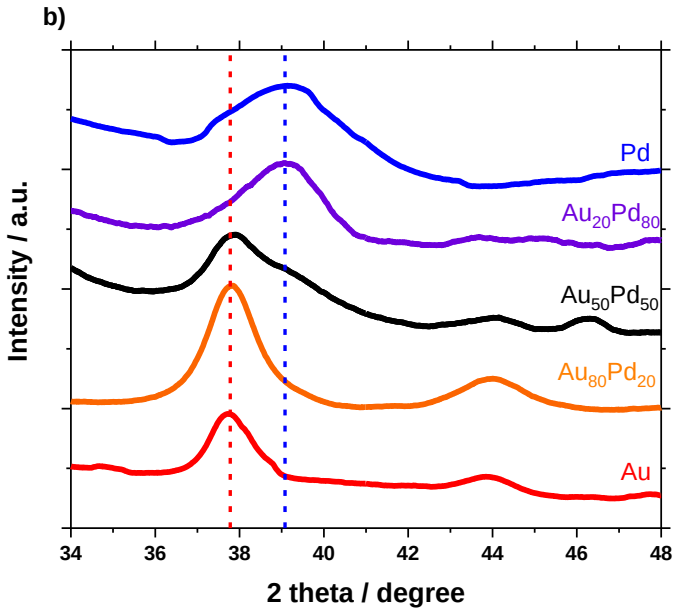


**Figure S5**. (a) Reference XRD diffractograms for fcc Au and Pd. (b) Example of spectrum focusing on the (111) peak position for various samples, as indicated.

The poor resolution of the diffractograms is attributed to the relatively low amount of material available for the measurement and the small size of the NPs. Note that due to this issue each diffractogram was adjusted with different factors to be plotted on the same Y-axis.

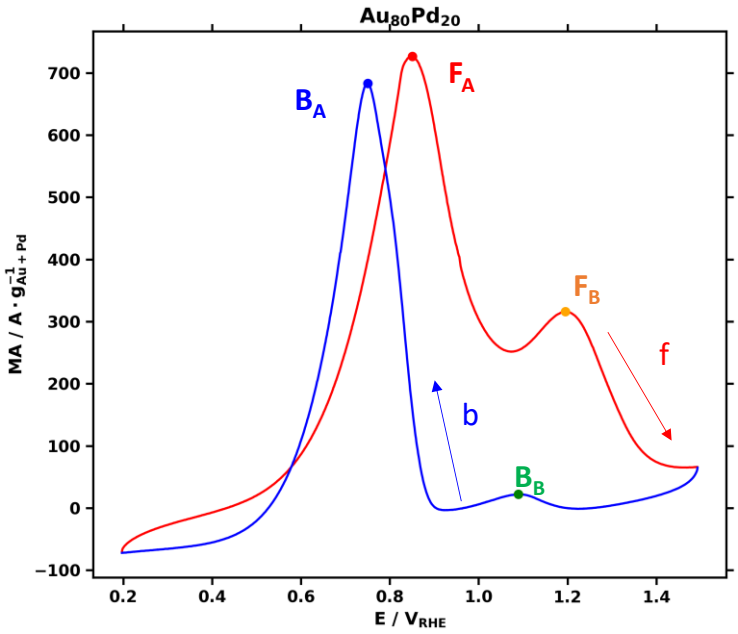


**Figure S6**. Example of CV recorded in 1 M KOH and 1 M Ethanol at a scan rate of 50 mV $s^{-1}$ for $Au_{80}Pd_{20}$ sample. The points indicated are those used for the characterization of the samples, see also the section metrics in **section 5**.

In **Figure S6**, the red part of the CV correspond to the forward (F or f) scan from low to high potentials whereas the blue part of the CV correspond to the backward (B or b) scan from high to low potentials. The higher intensity in the forward scan ($F_A$) corresponds to the oxidation of the ethanol for sites with lower overpotentials (likely Pd sites) whereas the backward oxidative peak ($B_A$) is attributed to the cleaning of the surface after the oxidative scan.[18] The counterpart labelled with a B are the same but attributed to Au sites.[20] Unless otherwise specified, the MA was evaluated at the point $F_A$. The ratio of the intensity at $F_A$ and $B_A$ (alternatively $F_B$ and $B_B$) is a common metric to give an indication of the poisoning resistance of the material.[18,20] The higher the $I_f/I_b$ ratio, the more resistance to poisoning the material is expected to be.

**A)**

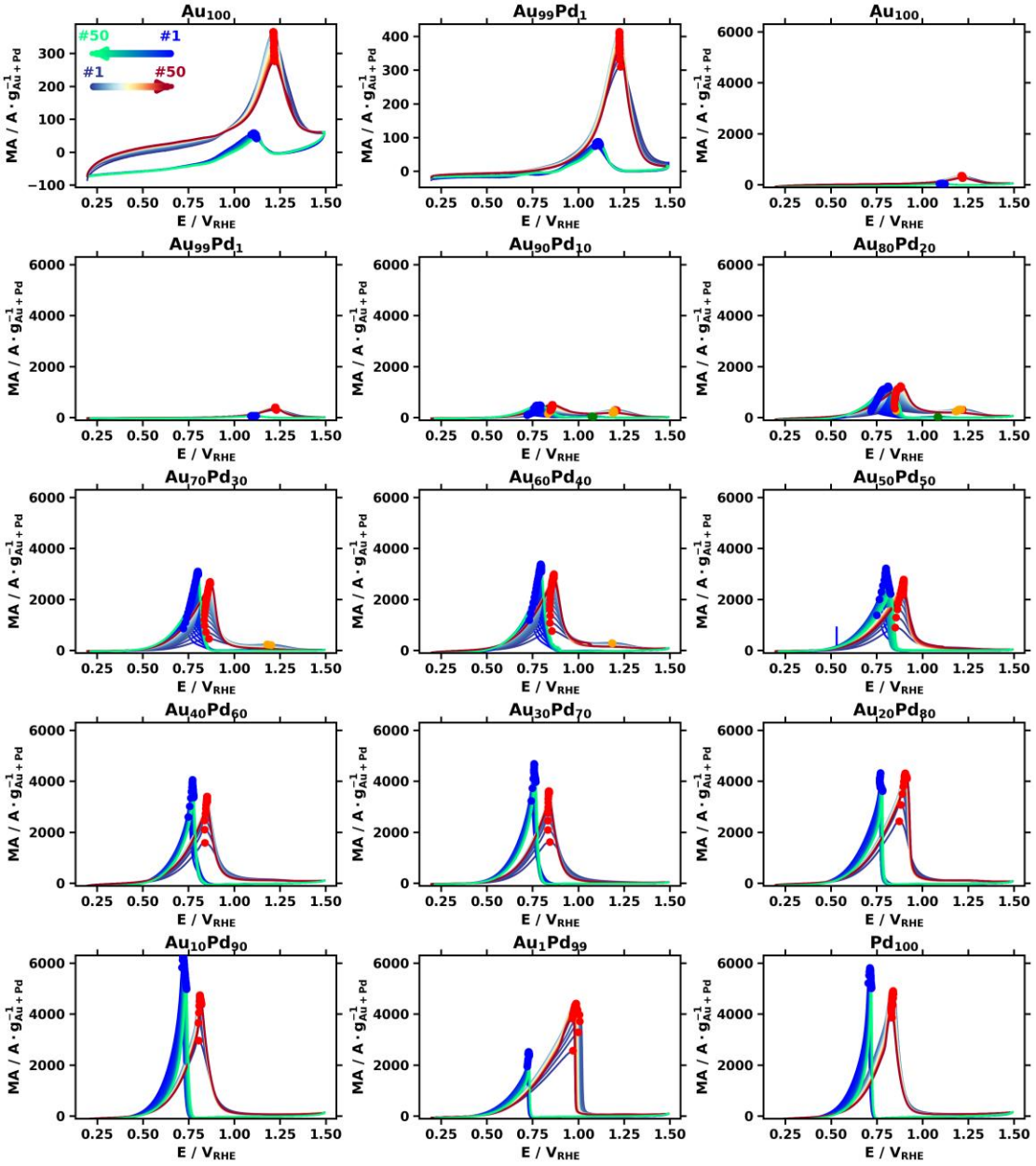
Au100
Au99Pd1
Au100
Au99Pd1
Au90Pd10
Au80Pd20
Au70Pd30
Au60Pd40
Au50Pd50
Au40Pd60
Au30Pd70
Au20Pd80
Au10Pd90
Au1Pd99
Pd100
#50
#1
#1
#50
MA / A · g⁻¹Au + Pd
E / VRHE

B)

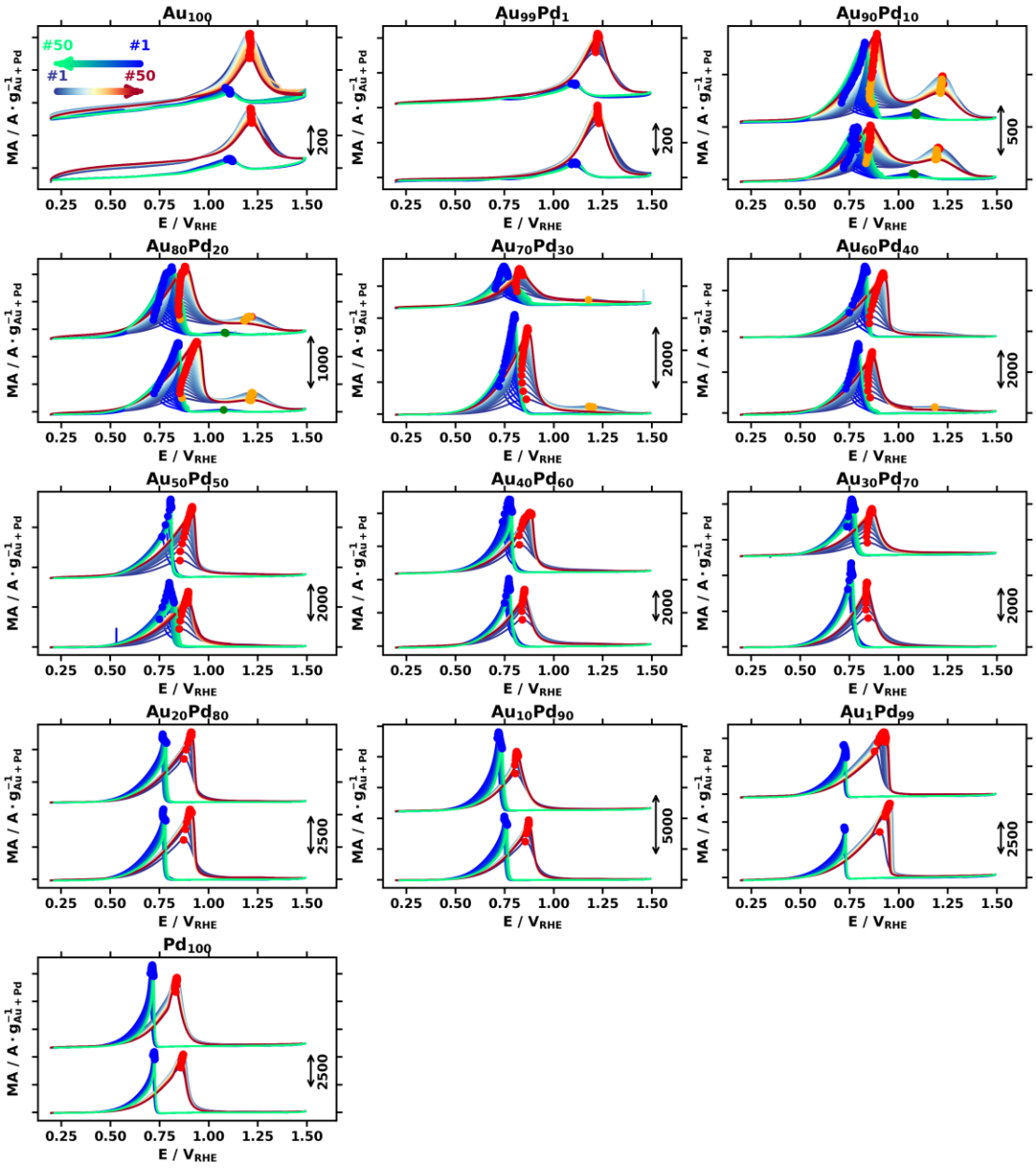


**Figure S7**. Illustrative CVs in 1 M KOH and 1 M Ethanol and at a scan rate of 50 mV $s^{-1}$ for various $Au_xPd_{1-x}$ samples, as indicated, a color code indicate the scan number from 1 to 50 for the forward and backward scans. (A) One or (B) two datasets for each composition are represented. As much as possible all CVs are reported with the same Y-axis range but for a better look at the two least active catalysts ($Au_{100}$ and $Au_{99}Pd_1$) a zoomed-in Y-axis is also provided in (A). In (B) are reported two datasets with an offset to give an idea of the reproducibility of the measurement whereas (A) only represents 1 dataset to better compare the different samples and their respective features between themselves.

**a)**

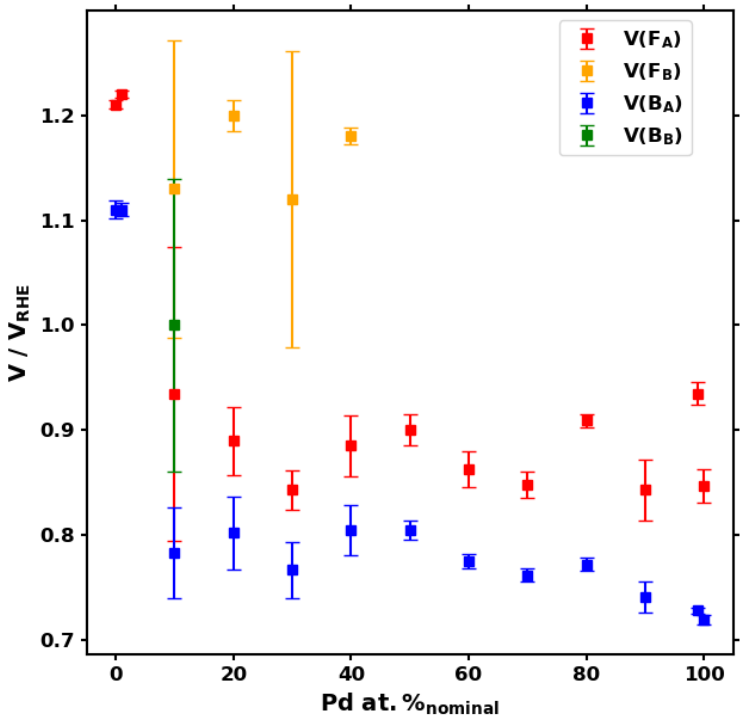
V(F$_A$)
V(F$_B$)
V(B$_A$)
V(B$_B$)
V / V$_{RHE}$
1.2
1.1
1.0
0.9
0.8
0.7
0
20
40
60
80
100
Pd at. %$_{nominal}$

**b)**

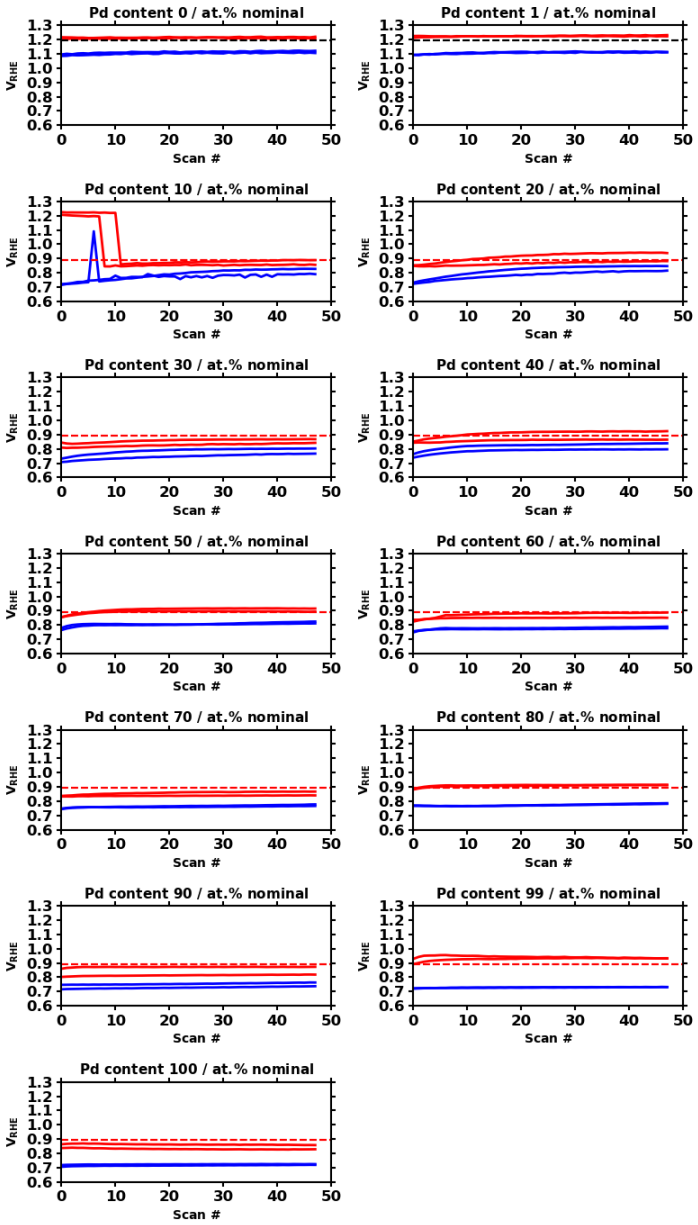


**Figure S8**. (a) Peaks position in $V_{RHE}$ as a function of the nominal composition of the sample. The color code corresponds to the code used in **Figure S6**. (b) Peaks position in $V_{RHE}$ as a function of the number of scan for different nominal compositions, as indicated. The color code corresponds to the code used in **Figure S6**. The dashed horizontal lines are a guide for the eyes at 0.9 $V_{RHE}$ or 1.2 $V_{RHE}$ (values used for CA, detailed below).

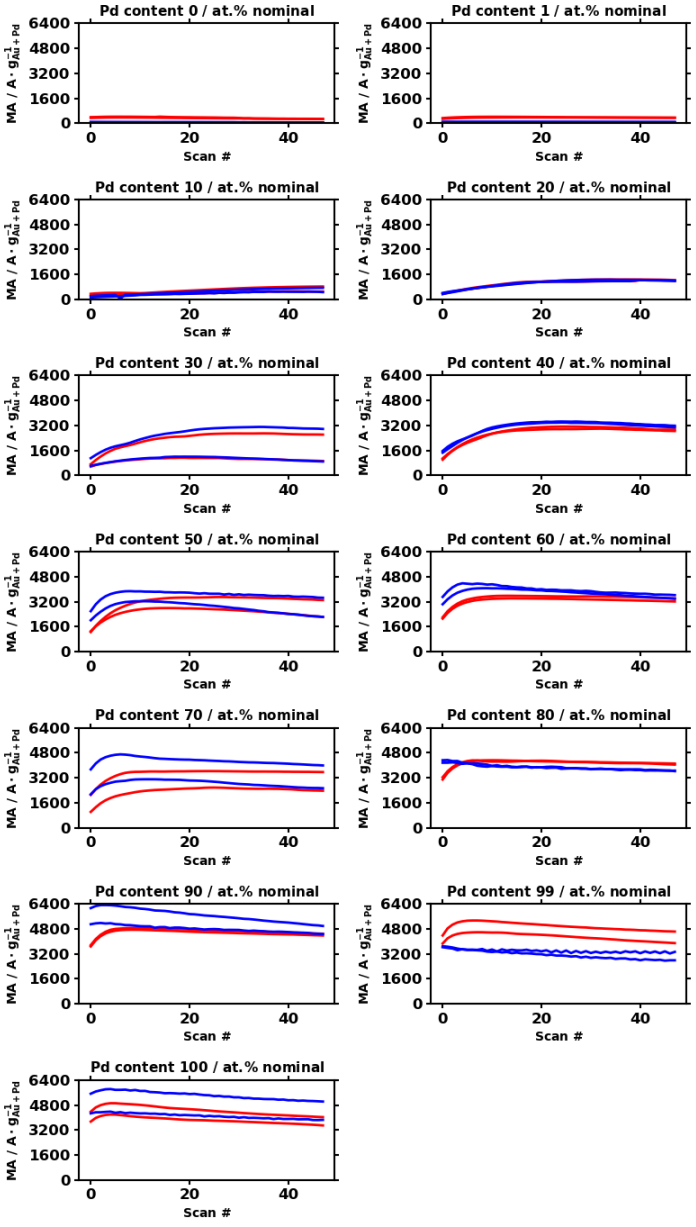


**Figure S9.** Evolution of the MA as a function of number of scans for the forward scan and backward scan for different nominal compositions, as indicated.

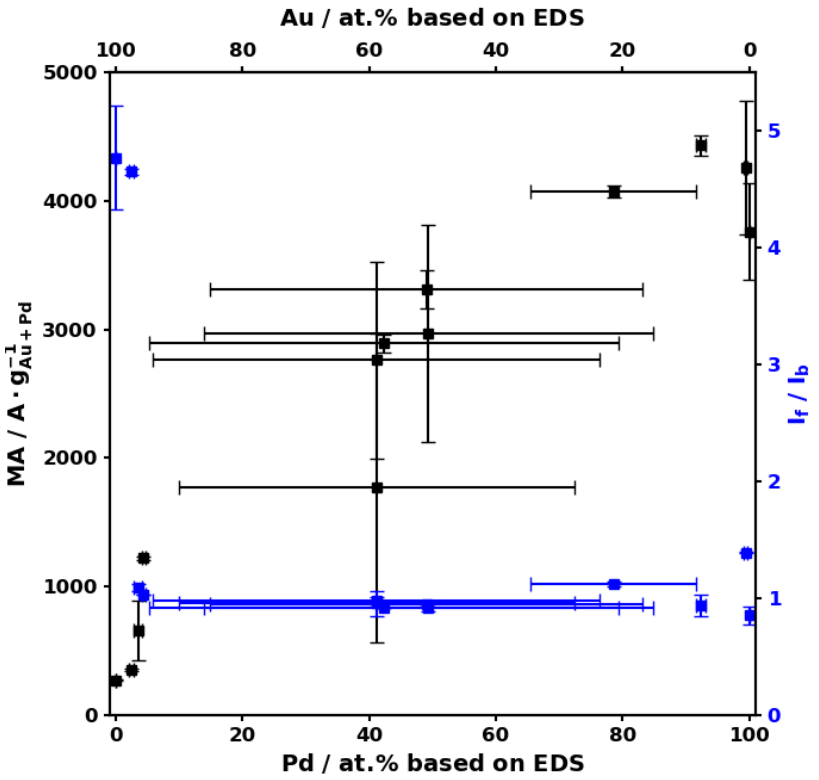


**Figure S10.** MA and $I_f/I_b$ ratio as a function of the experimental composition of the $Au_xPd_{1-x}$ samples retrieved from EDS. See discussion of **Figure 2** in the main manuscript.

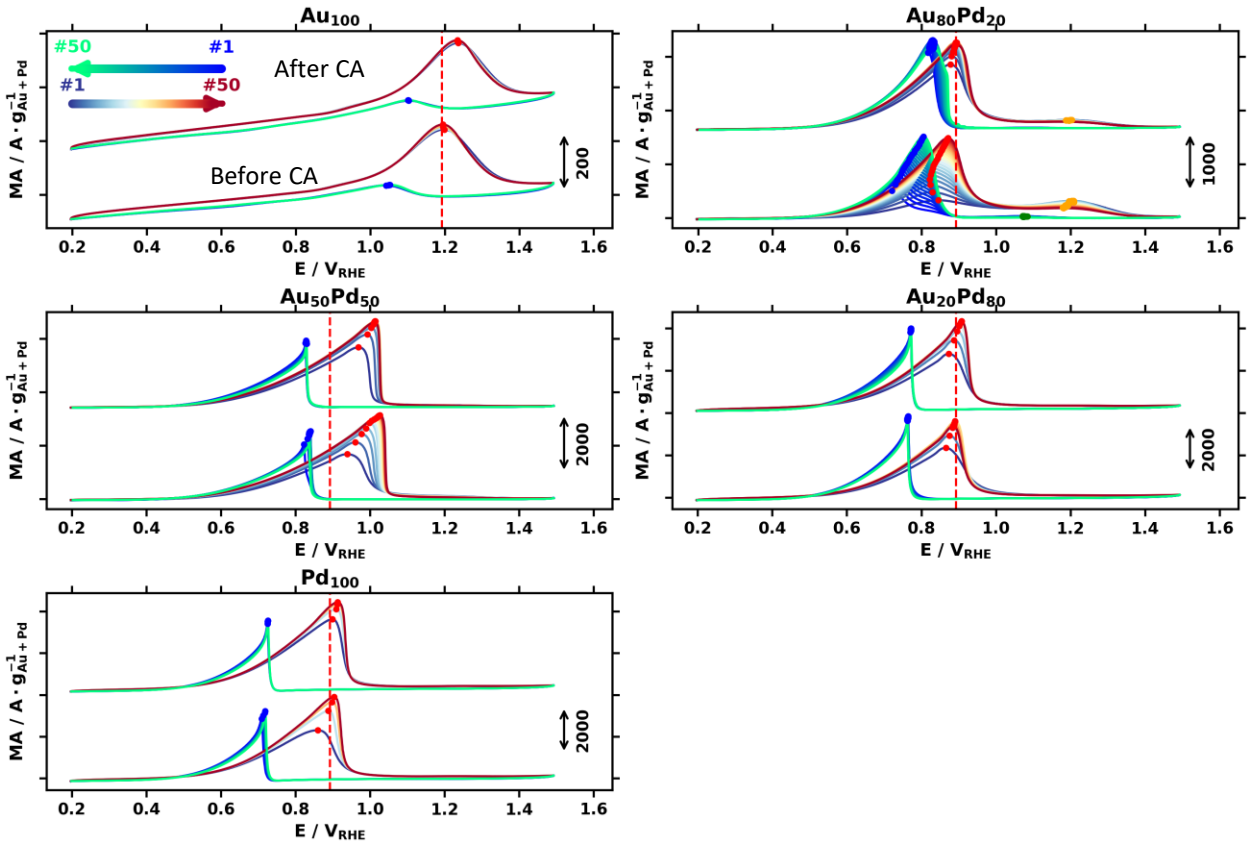


**Figure S11.** Illustrative CVs for various samples, before and after CA, as indicated. Two different datasets are represented in each panel: one before (bottom) and one after (top) CA. The voltage at which the CA was performed is represented by the vertical dashed red line.

# References


1 Van Hyning, D. & Zukoski, C. Formation mechanisms and aggregation behavior of borohydride reduced silver particles. *Langmuir* **14**, 7034-7046 (1998). https://doi.org/10.1021/la980325h

2 Deraedt, C. *et al.* Sodium borohydride stabilizes very active gold nanoparticle catalysts. *Chemical Communications* **50**, 14194-14196 (2014). https://doi.org/10.1039/c4cc05946h

3 Iqbal, M. *et al.* Preparation of gold nanoparticles and determination of their particles size via different methods. *Materials Research Bulletin* **79**, 97-104 (2016). https://doi.org/10.1016/j.materresbull.2015.12.026

4 Elnagar, M. *et al.* Water-soluble ionic carbon nitride as unconventional stabilizer for highly catalytically active ultrafine gold nanoparticles. *Nanoscale* **15**, 19268-19281 (2023). https://doi.org/10.1039/d3nr03375a

5 Larm, N. *et al.* Role of Heavy Water in the Synthesis and Nanocatalytic Activity of Gold Nanoparticles. *ACS Nanoscience Au* **5**, 52-59 (2025). https://doi.org/10.1021/acsnanoscienceau.4c00069

6 Andersen, K. J. *et al.* Positive Thinking: Countercation Effects in Colloidal Syntheses of Gold Nanoparticles. *Nano Letters* **25**, 42, 15436–15442 (2025). https://doi.org/10.1021/acs.nanolett.5c04815

7 Sørensen, M. P. *et al.* Room temperature surfactant-free syntheses of colloidal gold nanoparticles: comparison of the precursors $HAuCl_4$ and $HAuBr_4$. *Colloids and Surfaces A: Physicochemical and Engineering Aspects* **739**, 140023 (2025). https://doi.org/10.26434/chemrxiv-2025-l8w54

8 Fokam, H. K., Smolska, A. & Quinson, J. Surfactant-free $NaBH_4$-mediated synthesis of gold nanoparticles in water at room temperature: fine size control for active nanocatalysts. *ChemRxiv* **Preprint** (2025). https://doi.org/10.26434/chemrxiv-2025-rwh33

9 Fokam, H. K., Smolska, A. & Quinson, J. $NaBH_4$-mediated syntheses of colloidal gold nanocatalysts in water: are additives really needed? *ChemRxiv* **Preprint** (2025). https://doi.org/10.26434/chemrxiv-2025-h0hpb

10 Kettemann, F. *et al.* Reliable palladium nanoparticle syntheses in aqueous solution: the importance of understanding precursor chemistry and growth mechanism. *CrystEngComm* **17**, 1865-1870 (2015). https://doi.org/10.1039/c4ce01025f

11 Ipadeola, A. *et al.* Unveiling the effect of shapes and electrolytes on the electrocatalytic ethanol oxidation activity of self-standing Pd nanostructures. *Heliyon* **9**, e16890 (2023). https://doi.org/10.1016/j.heliyon.2023.e16890

12 Wuithschick, M., Witte, S., Kettemann, F., Rademann, K. & Polte, J. Illustrating the formation of metal nanoparticles with a growth concept based on colloidal stability. *Physical Chemistry Chemical Physics* **17**, 19895-19900 (2015). https://doi.org/10.1039/c5cp02219c

13 Anantharaj, S., Jayachandran, M. & Kundu, S. Unprotected and interconnected $Ru^0$ nano-chain networks: advantages of unprotected surfaces in catalysis and electrocatalysis. *Chemical Science* **7**, 3188-3205 (2016). https://doi.org/10.1039/c5sc04714e

14 Charde, R. P., van Devener, B. & Nigra, M. M. Surfactant- and Ligand-Free Synthesis of Platinum Nanoparticles in Aqueous Solution for Catalytic Applications. *Catalysts* **13**, 246 (2023). https://doi.org/10.3390/catal13020246

15 Larm, N. E., Thon, J. A., Vazmitsel, Y., Atwood, J. L. & Baker, G. A. Borohydride stabilized gold-silver bimetallic nanocatalysts for highly efficient 4-nitrophenol reduction. *Nanoscale Advances* **1**, 4665-4668 (2019). https://doi.org/10.1039/c9na00645a

16 Quinson, J. Room Temperature Surfactant-Free Syntheses of Gold Nanoparticles in Alkaline Mixtures of Water and Alcohols: A Model System to Introduce Nanotechnology and Green Chemistry to Future Chemists and Engineers. *Journal of Chemical Education* **100**, 3612-3619 (2023). https://doi.org/10.1021/acs.jchemed.3c00492

17 Larsen, R., Villadsen, T. L., Mathiesen, J. K., Jensen, K. M. Ø. & Bøjensen, E. D. NP-SAM: Implementing the Segment Anything Model for Easy Nanoparticle Segmentation in Electron Microscopy Images. *ChemRxiv* (2023). https://doi.org/10.26434/chemrxiv-2023-k73qz-v2

18 Panagopoulos, D., Asghari Alamdari, A. & Quinson, J. Surfactant-free colloidal gold nanoparticles: room temperature synthesis, size control and opportunities for catalysis. *Materials Today Nano* **29**, 100600 (2025). https://doi.org/10.1016/j.mtnano.2025.100600

19 Kawashima, K. *et al.* Accurate Potentials of Hg/HgO Electrodes: Practical Parameters for Reporting Alkaline Water Electrolysis Overpotentials. *ACS Catalysis*, 13, 1893-1898 (2023). https://doi.org/10.1021/acscatal.2c05655

20 Quinson, J. *et al.* Surfactant-free colloidal syntheses of gold-based nanomaterials in alkaline water and mono-alcohol mixtures. *Chemistry of Materials* **35**, 2173–2190 (2023). https://doi.org/10.1021/acs.chemmater.3c00090

21 Yaqoob, L., Noor, T. & Iqbal, N. A comprehensive and critical review of the recent progress in electrocatalysts for the ethanol oxidation reaction. *RSC Advances* **11**, 16768-16804 (2021). https://doi.org/10.1039/d1ra01841h

22 Feng, Y. Y. *et al.* Highly active PdAu alloy catalysts for ethanol electro-oxidation. *Journal of Power Sources* **232**, 99-105 (2013). https://doi.org/10.1016/j.jpowsour.2013.01.013

23 Silva, L. S. R. *et al.* AuPd/C core-shell and alloy nanoparticles with enhanced catalytic activity toward the electro-oxidation of ethanol in alkaline media. *Applied Catalysis B-Environmental* **251**, 313-325 (2019). https://doi.org/10.1016/j.apcatb.2019.03.067